ACS APPLIED MATERIALS & INTERFACES

Research Article

www.acsami.org

Improved Efficiency and Stability of Polymer Solar Cells Utilizing Two-Dimensional Reduced Graphene Oxide: Graphene Oxide Nanocomposites as Hole-Collection Material

Lei Chen,[†] Donghe Du,[†] Kuan Sun,[†] Jianhui Hou,[‡] and Jianyong Ouyang*,[†]

[†]Department of Material Science and Engineering, National University of Singapore, Singapore 117574

[‡]Institute of Chemistry, Chinese Academy of Sciences, Beijing, China

ABSTRACT: Improving device efficiency and stability of polymer solar cells (PSCs) is crucial for their practical application. Although graphene oxide (GO) could replace the poly(3,4-ethylenedioxythiophene):poly(styrenesulfonate) (PEDOT:PSS) as the hole-collection material and improve the photovoltaic stability of PSCs, the power conversion efficiency is moderate because of its insulating nature. In this article, nanocomposites of two-dimensional reduced graphene oxide (rGO) and GO are used to replace the acidic PEDOT:PSS as the hole-collection material of PSCs. The nanocomposites are formed by dispersing rGO into aqueous solution of GO. GO serves as a surfactant, and it can stabilize rGO. The presence of rGO can quench the photoluminescence of GO in water. The nanocomposite films exhibit higher conductivity than GO films without rGO. They are used as the hole-collection material of PSCs. The optimal PSCs with poly(3-hexylthiophene) and [6,6]-phenyl-C61-butyric acid methyl ester exhibit such photovoltaic performances: short-circuit current density of 10.37 mA cm^{-2}, open-circuit voltage of 0.60 V, fill factor of 67.66%, and power conversion efficiency of 4.21%. The photovoltaic efficiency is much higher than that of the control devices with GO only (3.36%) as the hole-collection material. In addition, the presence of rGO in GO gives rise to better stability for the PSCs in air than that of the devices with GO only. The devices with rGO:GO composites as the hole-collection materials exhibit much better stability in power conversion efficiency than the control devices with PEDOT:PSS.

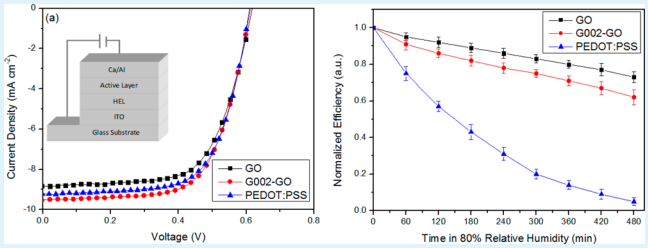

KEYWORDS: *polymer solar cells, hole collection, reduced graphene oxide, graphene oxide*

1. INTRODUCTION

Bulk-heterojunction polymer solar cells (PSCs) are regarded as the next-generation solar cells because they have the advantages of low cost and high mechanical flexibility. The power conversion efficiency (PCE) has been continuously improved. PCEs exceeding 9% and 10% have been reported for single[1] and tandem PSCs,[2,3] respectively. Besides the synthesis of new donor[4−12] and acceptor materials[13−15] and optimization of the active layer morphology,[5,16−19] the interfaces between the electrodes and the active layer also play a pivotal role in the light-to-electricity conversion process.[20−30] Conductivity, transparency, solution processability, film morphology, and stability are key factors for selecting the interfacial materials for PSCs. Although poly(3,4-ethylenedioxythiophene):poly(styrenesulfonate) (PEDOT:PSS) is the most popular hole-collection material, it is acidic and hygroscopic, which causes the corrosion to the indium tin oxide (ITO) anode and poor stability for PSCs.[31−33] Both device performance and stability are important for the practical application of PSCs. Therefore, it is important to develop new cost-efficient and solution-processable hole-collection interfacial materials. Although metallic oxides, such as MoO_3,[34] V_2O_5,[35,36] NiO_x,[37] and WO_3,[38,39] by solution processing were demonstrated as the hole-collection materials of PSCs, the fabrication conditions have to be well-controlled to have the suitable thickness and morphology. In addition, these oxides have poor mechanical flexibility.

Recently, graphene oxide (GO) and its derivatives were also investigated as a hole-collection material of PSCs.[40−49] GO is a two-dimensional material. It has a work function of about 4.9 V, almost the same as that of PEDOT:PSS, and it can be dispersed in water. GO can give rise to much better stability for PSCs than PEDOT:PSS.[48] However, GO is an insulator and leads to a high internal resistance for PSCs, which lowers the short-circuit current density (J_{sc}) and fill factor (*FF*). To improve the conductivity, chemical and physical methods have been exploited to modify GO, such as moderately reduced GO treated with *p*-TosNHNH$_2$ (*pr*-GO),[49] thermal annealing of GO,[50] sulfonation of GO (GO-OSO$_3$H),[51] and blending with a large amount of (~20 wt %) conductive single-walled carbon nanotubes (SWCNT).[52] However, *p*-TosNHNH$_2$ is a highly toxic reductant. The product must be further purified after treatment. High temperature up to 230 °C is required for thermal annealing treatment. GO-OSO$_3$H with higher acidity

Received: September 15, 2014
Accepted: November 21, 2014
Published: November 21, 2014

compared to GO may erode the ITO anode and result in poor device stability as PEDOT:PSS hole-collection layer. Addition of a large quantity of costly SWCNT will lead to increased production costs.

In this work, we report that highly reduced GO (rGO) powders can be dispersed and stabilized in water using GO as surfactant by simple sonication treatment. Nanocomposites of two-dimensional rGO and GO were readily obtained and applied as the hole-collection layer (HCL) of PSCs. A minuscule amount of rGO additive (2 wt % with respect to GO) could significantly improve the vertical conductivity of GO-based HCL. Employing this nanocomposite as HCL, the optimal PSCs with poly(3-hexylthiophene) (P3HT) and [6,6]-phenyl-C_{61}-butyric acid methyl ester (PCBM) exhibit a power conversion efficiency of 4.21%. The PCE is much higher than that of the control devices with GO only as the HCL (3.36%) and comparable to the PEDOT:PSS-based device (4.04%). More importantly, utilization of this two-dimensional nanocomposites does not affect the chemical properties of GO matrix, giving rise to much better stability for the devices than that with PEDOT:PSS as hole-collection material.

2. RESULT AND DISCUSSION

2.1. Preparation and Characterization of G_x-GO Nanocomposites. Highly reduced GO shows good conductivity but poor solution processability. GO can be well-dispersed in water due to the existence of hydroxyl and carboxyl groups. It can behave as a surfactant because of the hydrophobic domains and hydrophilic units.[53] Herein, rGO was directly dispersed in GO aqueous solution to obtain the rGO:GO nanocomposites by ultrasonication, which is denoted as G_x-GO, where x is the percentage of rGO with respect to GO.

Figure 1 shows pictures of aqueous solutions dispersed with 0.5 g L^{-1} GO, 0.5 g L^{-1} G002-GO (the loading of rGO is 2 wt

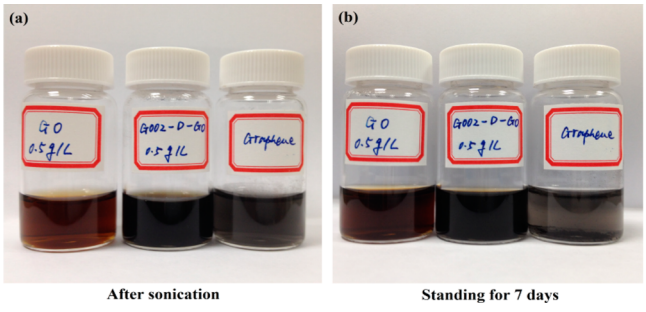

Figure 1. Photographs of (a) freshly prepared GO, G002-GO, and rGO solutions and (b) 7 days after the solution preparation.

% with respect to GO), and 0.01 g L^{-1} rGO (the same rGO concentration as that in G002-GO). The rGO is completely dispersed in the GO aqueous solution. The solution of GO and rGO has good stability. No obvious rGO particle was observed after ultrasonication and even 7 days after the solution preparation. In contrast, rGO cannot be completely dispersed in water in the absence of GO. After 7 days, a large amount of precipitates appeared at the bottom of the solution. The rGO is stabilized by GO in water. GO has hydrophobic domains and hydrophilic units, and it is considered as a two-dimensional surfactant.[52] In a stable dispersion, the hydrophobic rGO sheets should be surrounded with the hydrophilic GO sheets in water. It is expected that $\pi-\pi$ coupling can take place between GO and rGO sheets because GO has conjugated domains.

The interaction between GO and rGO sheets was explored by photoluminescence spectroscopy. As shown in Figure 2,

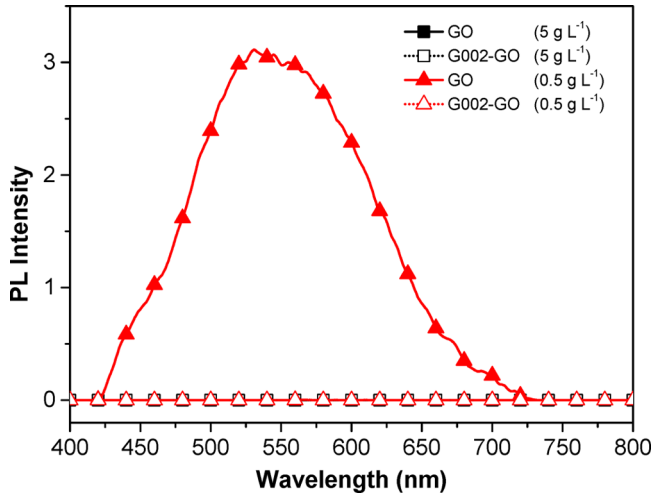

Figure 2. Photoluminescent spectra of GO (solid line) and G002-GO (dotted line) solution with different concentrations.

when the GO concentration was 5.0 g L^{-1}, no fluorescence was detected for both GO and G002-GO solutions. It can be attributed to the concentration quenching of GO.[54] When the GO concentration was lowered to 0.5 g L^{-1}, remarkable photoluminescence was observed in the wavelength range from 420 to 720 nm. The presence of 0.01 wt % rGO almost completely quenched the photoluminescence of the solution of 0.5% GO. As rGO is in metallic state, it can quench the photoluminescence of the insulating GO in its vicinity. This confirms the interaction between rGO and GO in water.

The composition of G_x-GO with different rGO content was investigated by X-ray photoelectron spectroscopy (XPS). Films of G_x-GO nanocomposites were prepared by drop casting the mixture solutions on the silicon wafers and dried at 60 °C in an oven overnight. The weight loadings of rGO are 0%, 2%, and 10% with respect to GO in solution. In terms of the XPS results, the atomic ratios of carbon to oxygen are 2.76:1, 2.88:1, and 3.69:1 for GO, G002-GO, and G010-GO, respectively. The C 1s XPS signal can be deconvoluted into three XPS bands at 284.5, 286.6, and 288.5 eV (Figure 3).[55] They correspond to C−C, C−O, and C═O structures. The ratios of the C−C integrated intensity to the total integrated intensity of C−O and C═O structures are 1.16:1, 1.20:1, and 1.50:1 for pure GO, G002-GO, and G010-GO. This is consistent with the rGO loading in these samples.

Atomic force microscopic (AFM) images (Figure 4) were acquired to study the surface morphology of G_x-GO films prepared on silicon wafer by spin coating. The two-dimensional sheets can be observed. The film thickness is around 3 nm, which is corresponding to two- or three-layer GO sheets. The surface roughnesses are 0.860, 0.793, and 0.967 nm for GO, G002-GO, and G010-GO films, respectively. The presence of rGO hardly affects the roughness of the films.

It should be noted that the AFM images were taken only in a small area for the very thin G_x-GO films. We also investigated the surface morphology of G_x-GO films on silicon in a larger area by scanning electron microscope (SEM). Since the

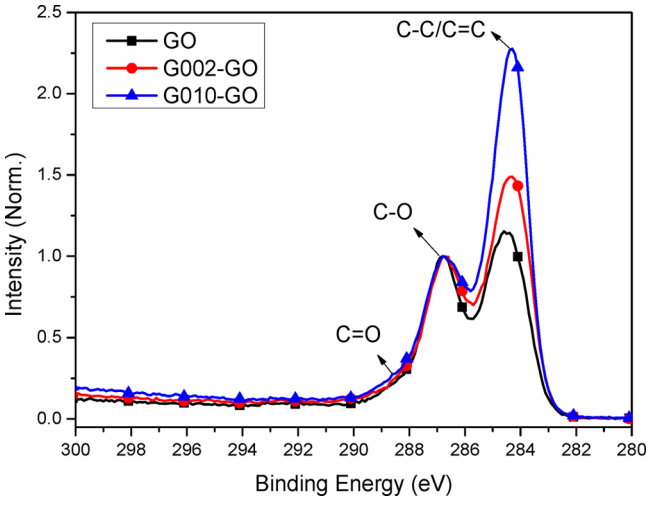

Figure 3. XPS spectra of GO, G002-GO, and G010-GO.

samples prepared by spin coating are too thin to obtain clear images, samples of GO, G002-GO, and G010-GO on silicon wafer were prepared by drop-casting. As shown in Figure 5, it was found that the presence of rGO could significantly affect the surface morphology of the thick films to form starburst-like patterns. This is consistent with the stabilization of rGO by GO in water. The rGO sheets act as the central part, and they are surrounded with GO sheets.

2.2. Polymer Solar Cells with G_x-GO Composites as the Hole-Collection Material. G_x-GO composites films were used as the HCL of polymer solar cells with a device configuration of ITO/HCL/P3HT:PCBM/Ca/Al. They were prepared on ITO/glass substrate by spin coating and had a thickness of around 3 nm. Control devices with GO only or PEDOT:PSS for the HCL were also fabricated. The photovoltaic performances of these devices were summarized in Table 1.

The device with GO only as the HCL exhibits a open-circuit voltage (V_{oc}) of 0.60 V, J_{sc} of 9.65 mA cm^{-2}, *FF* of 58.03%, and moderate PCE of 3.36% under AM1.5G illumination. Adding 1 wt % rGO increases J_{sc} to 9.98 mA cm^{-2} and *FF* to 60.79%, while it does not affect the V_{oc} value. The optimal rGO loading is 2 wt % in the composite film in terms of the photovoltaic performance of the devices. The optimal PCE is 4.21%. Further increase in the rGO loading lowers the J_{sc}, *FF*, and PCE of PSCs. The optimal rGO loading is 2 wt % in the composite film in terms of the photovoltaic performance of the devices. This is much lower than the optimal SWCNT loading in GO.[52] This might be caused by the dimensionality of the adducts. Carbon nanotubes are one-dimensional materials, while rGO has a two-

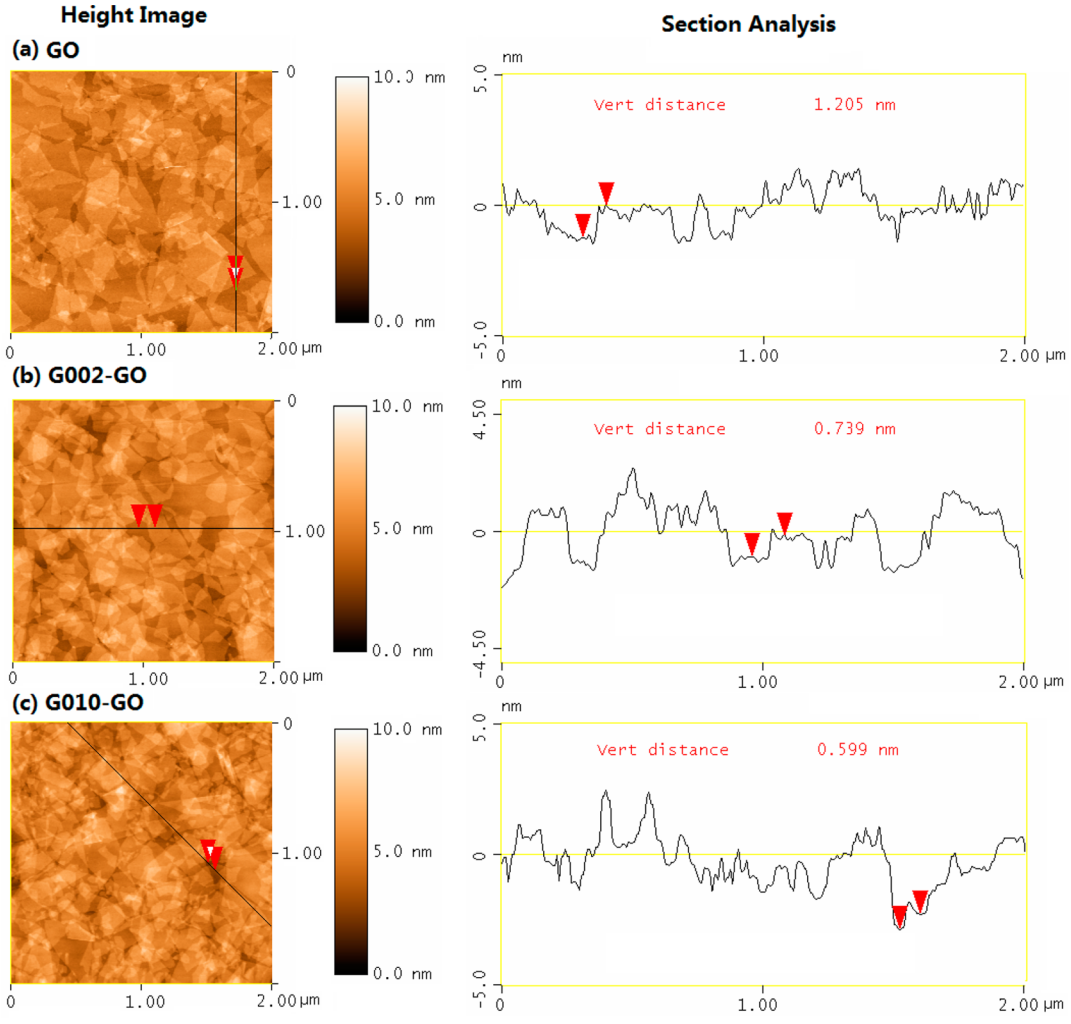

Figure 4. AFM height images and section analysis of spin-coated GO (a), G002-GO (b), and G010-GO (c) on silicon wafer.

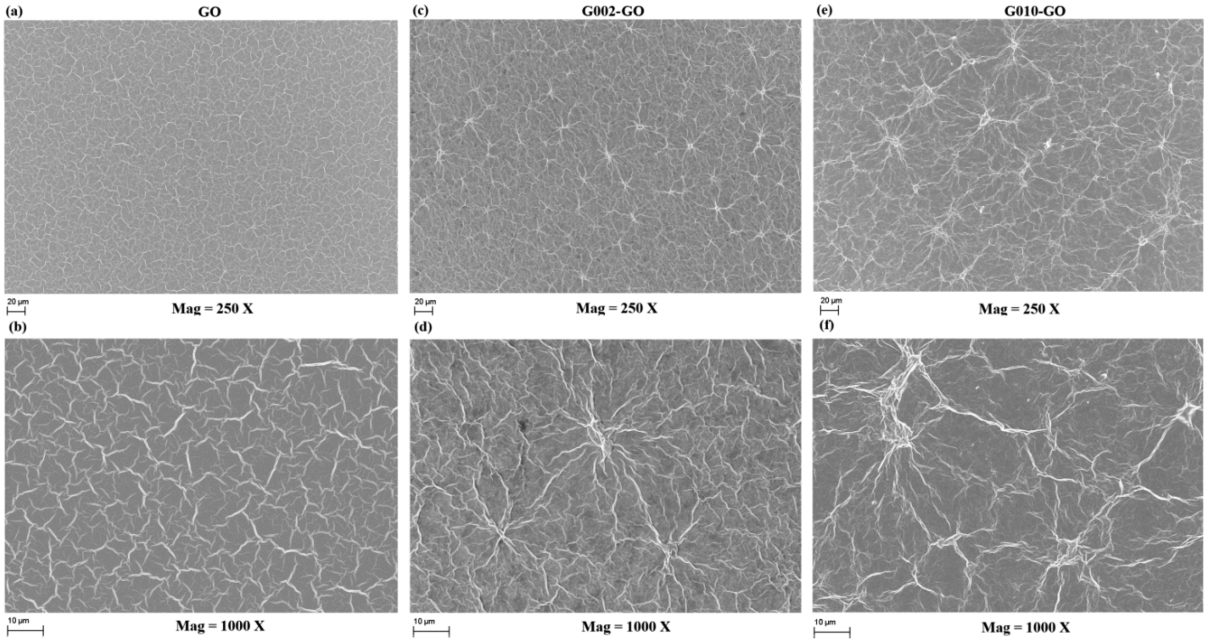

Figure 5. SEM images of drop-casted GO (a, b), G002-GO (c, d), and G010-GO (e, f) on silicon wafer under two different magnifications.

Table 1. Photovoltaic Performances of PSCs with GO, G_x-GO, and PEDOT:PSS as the HCL

device	HCL	V_{oc} [V]	J_{sc} [mA cm^{-2}]	*FF* [%]	*PCE* [%][a]	R_s [Ω cm^2]	R_{sh} [kΩ cm^2]
1	GO	0.60	9.65	58.03	3.36 (3.20 ± 0.14)	11.29	362.86
2	G001-GO	0.60	9.98	60.79	3.64 (3.43 ± 0.16)	3.49	185.89
3	G002-GO	0.60	10.37	67.66	4.21 (3.98 ± 0.18)	3.82	78.13
4	G003-GO	0.60	10.26	64.81	3.99 (3.72 ± 0.15)	4.34	16.75
5	G004-GO	0.60	9.86	62.04	3.67 (3.36 ± 0.25)	8.54	2.39
6	PEDOT:PSS	0.60	10.05	67.00	4.04 (3.92 ± 0.08)	3.70	312.24

[a]In the brackets are the average PCE values and standard deviations according to ten devices.

dimensional structure. The two-dimensional rGO provides more active surface area to facilitate the charge tunnel through the GO layer than the one-dimensional carbon nanotubes.

The control device using PEDOT:PSS as HCL shows almost the same V_{oc} and *FF* as the device of G002-GO, but with slightly lower J_{sc} (10.05 mA cm^{-2}) and PCE (4.04%) values. Figure 6a,b presents the *J*−*V* curves and external quantum efficiency (EQE) spectra of devices employing GO, G002-GO, and PEDOT:PSS as hole-collection materials. The device of G002-GO shows improved EQE value in a broad wavelength range from 350−650 nm, indicating more efficient charge collection.

Although the devices with G002-GO or PEDOT:PSS as the hole-collection material exhibit comparable PCEs, the former devices are much more stable than the latter. As shown in Figure 6c, the PCE of the PSCs with PEDOT:PSS rapidly decreases in ambient condition with humidity around 80%. After 8 h, the PCE becomes almost zero. This is related to the hygroscopic nature of PEDOT:PSS.[56] In contrast, the PCE of the devices with G002-GO is quite stable. The PCE is around 73% of the original efficiency after the same time span. Besides the hydroscopic difference of the materials, the ion diffusion may also affect the stability.[57] PEDOT:PSS can release protons particularly after it absorbs water. Interestingly, the devices with G002-GO shows even better stability in air than those with GO only. Presumably, this is related to the hydrophobic nature of rGO.

The presence of rGO in GO can increase J_{sc} and FF of PSCs. Since rGO is highly conductive, it lowers the vertical resistance of the hole-collection layer. However, the conductivity of the G_x-GO samples is not high enough for the measurement of their conductivity by the four-point probe technique. Thus, the current density−voltage curves of the structures with a GO, G_x-GO, or PEDOT:PSS film sandwiched between Al and ITO electrodes were tested to understand their different conductive properties. As shown in Figure 7, the addition of rGO into the GO films increases the current density. The current density becomes higher with rGO loading. The current density through the G002-GO film is even higher than that through the PEDOT:PSS film. Although the PEDOT:PSS film is much thicker than the G002-GO film, these are the thicknesses for these materials in the optimal PSCs. The current densities along the vertical direction are consistent with the J_{sc} values of the devices with G002-GO and PEDOT:PSS as the hole-collection materials.

The transmittance of the hole-collection layer can also affect J_{sc}. We inspected the optical transmittance of GO, G002-GO, and PEDOT:PSS film deposited on glass substrates (Figure 8). The addition of 2 wt % rGO only slightly decreases the transmittance of GO in the wavelength range shorter than 600 nm. Both the GO and G002-GO films show higher optical transmittance than that of PEDOT:PSS film when the wavelength is longer than 500 nm.

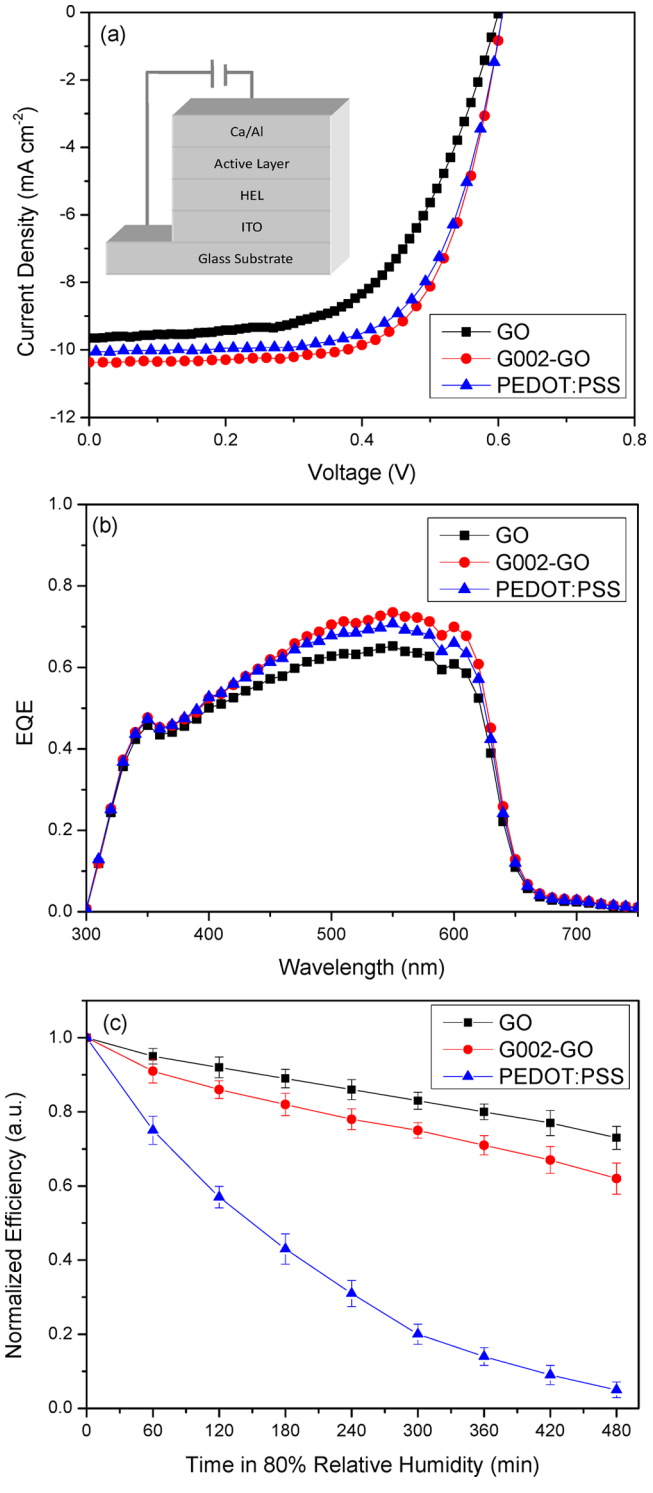

Figure 6. *J*–*V* curves under illumination (a) and EQE spectra (b) of PSCs with GO, G002-GO, and PEDOT:PSS as the hole-collection material. (c) Variation of power conversion efficiency with time for unencapsulated PSCs with different hole-collection materials in ambient condition with humidity around 80%.

Apart from the conductivity, the work function of the composite film should be considered for the device performance. The work function of ITO coated with a G_x-GO film was studied by ultraviolet photoelectron spectroscopy (UPS) (Figure 9).[58] The work function (φ) could be calculated by the following equation:

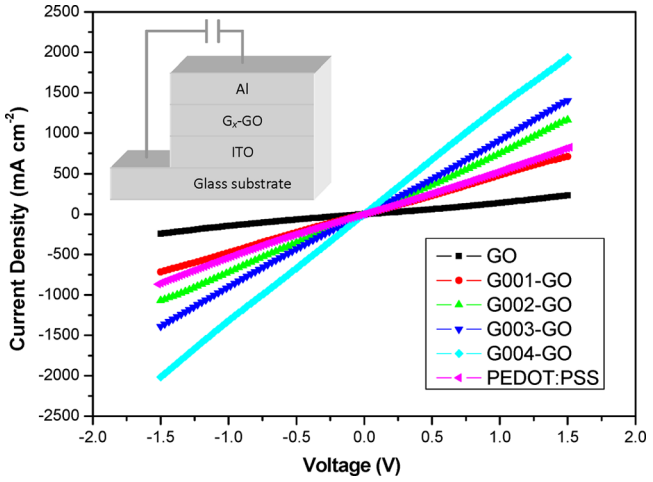

Figure 7. *J*–*V* curves of devices with a GO, G_x-GO, or PEDOT:PSS film sandwiched between ITO and Al. The thickness of the GO and G_x-GO films is around 3 nm, and the thickness of PEDOT:PSS is about 30 nm.

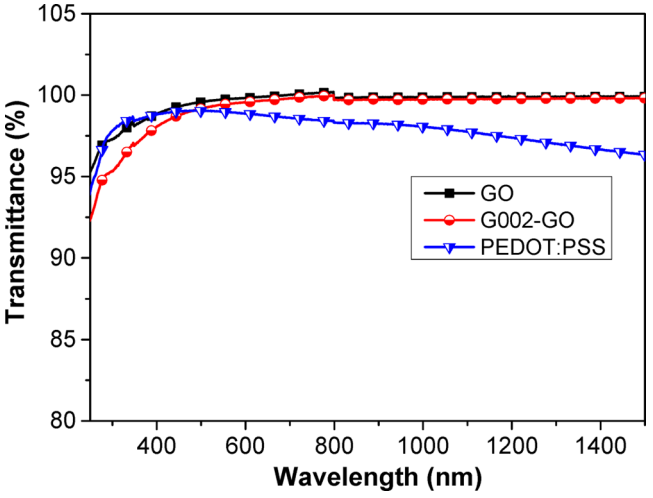

Figure 8. Optical transmittance of the GO (3 nm), G002-GO (3 nm), and PEDOT:PSS (30 nm) films. These are the optimal thicknesses for their application as the hole-collection material in PSCs.

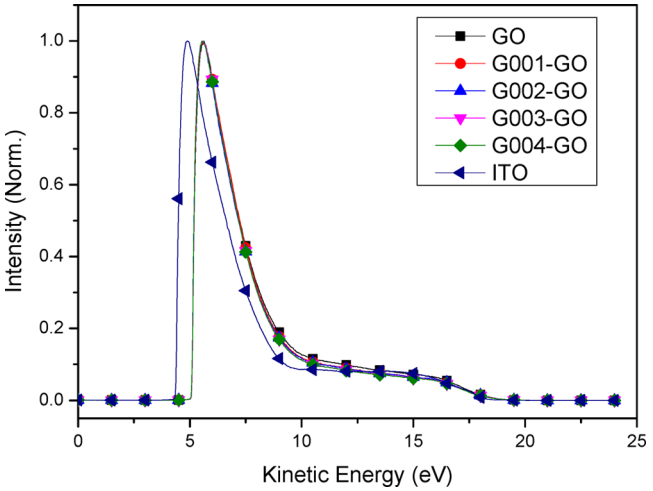

Figure 9. UPS spectra of bare ITO and ITO samples coated with GO and G_x-GO.

$$\varphi = h\nu + E_{\text{cutoff}} - E_{\text{F}} \quad (1)$$

where $h\nu$ is the photon energy of the UV source (He I light of 21.22 eV), E_{F} is the energy of the Fermi edge, and E_{cutoff} corresponds to the cutoff energy of the UPS spectrum. In comparison with bare ITO, the kinetic energy of the cutoff edge of ITO coated with a GO film shifts to a higher value by 0.67 eV. As the work function of ITO is about 4.5 eV, the work function of ITO/GO is about 5.2 eV. The highest occupied molecular orbital (HOMO) energy level of P3HT is around 5.0 eV. Thus, there is good energy level match for the hole collection. The presence of a small amount of rGO does not affect the kinetic energy of the cutoff edge. Hence, the work function factor can be excluded for the decrease of PCE when the rGO loading is higher than 2 wt % in G_x-GO.

We also calculated the series resistance (R_s) and shunt resistant (R_{sh}) according to the slopes at 1 and 0 V of the $J-V$ curve for the devices in dark (Table 1). The R_s value is 11.39 Ω cm^{-2} for the device with GO only. It decreases to 3.49 Ω cm^{-2} for the device based on the G001-GO layer. This is attributed to the lower vertical resistance of the G001-GO film. The series resistance then increases to 3.82, 4.34, and 8.54 Ω cm^{-2} for the devices with G002-GO, G003-GO, and G004-GO, respectively. The main impact of R_s is to influence the *FF* of the device. Enhanced R_s value at high rGO concentration leads to lower *FF* value. The R_{sh} value also changes after the addition of rGO into GO. It is 362.86 kΩ cm^{-2} for the device with GO only. It decreases to 185.89, 78.13, 16.75, and 2.39 kΩ cm^{-2} for the devices with G001-GO, G002-GO, G003-GO, and G004-GO, respectively. Lower R_{sh} suggests there is an alternate current path for the light-generated current. Such a diversion reduces the amount of current flowing through the solar cell junction, leading to lower J_{sc} value. The decrease in the R_{sh} might be due to the aggregation induced by rGO as observed by SEM.

Excessive rGO supplies another possible way for the current loss. GO can act as effective hole-extraction/electron-blocking materials because it has high work function (~5.0 eV) and large band gap (~3.6 eV). This hinders the electron transport from the lowest unoccupied molecular orbital (LUMO) of PCBM into the ITO anode.[41] However, the work function of graphene is 4.2−4.6 eV, which is similar to the LUMO level (~4.2 eV) of PCBM (Figure 10). When rGO is overloaded and cannot be shielded by GO, it will directly contact the active layer. In this case, electrons can transport from the LUMO of PCBM into the G_x-GO layer, leading to lower J_{sc} values. Therefore, there is an optimal rGO loading for the hole-collection layer of PSCs.

In a previous report,[41,52] the OPV device performance is quite sensitive to the thickness of the GO layer because of its insulating property. The optimal thickness for the GO film is around 3 nm, which corresponds to about two or three layers of GO nanosheets, in terms of the photovoltaic efficiency. Such a thin layer is unfavorable for the practical manufacture. The photovoltaic performance of PSCs becomes less sensitive to the thickness of the hole-collection layer in the presence of rGO. Devices with a thicker hole-collection layer were also fabricated by varying the GO concentrations in water, which were 2.0 and 2.5 mg mL^{-1}. The device performances are summarized in Table 2. Devices with thicker GO and G002-GO layers show obviously decreased *FF*. It can be ascribed to the higher R_s value, which is calculated to be 13.51, 6.16, 15.87, and 8.62 Ω cm^{-2} for devices 1, 2, 3, and 4, respectively. Although PCE of the PSCs with G002-GO decreases with thicker HCL, the dependence is less than that with GO only. The PCE drastically decreased to 2.69% with a 6 nm GO layer, while it still maintained a moderate efficiency of 3.48% with a 7 nm G002-GO layer. Apart from the conductive properties, the transmittance of the HCL layer can also affect the PCE. But that should be a minor factor because both rGO and GO are highly transparent in the visible range and the G_x-GO films are quite thin. This is also supported by the slight decrease in the J_{sc} value when the G_x-GO layer becomes thicker.

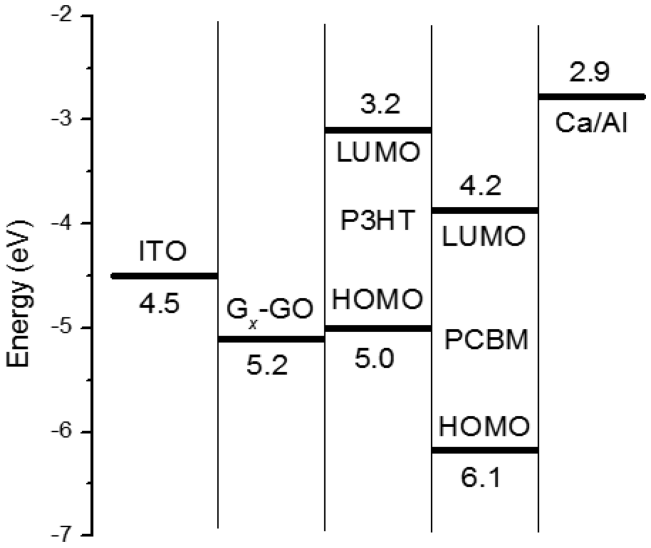

Figure 10. Energy level alignment of G_x-GO based photovoltaic device.

Table 2. Photovoltaic Performances of PSCs with Different Thickness GO and G002-GO Films as the HCL

device	HCL	V_{oc} [V]	J_{sc} [mA cm^{-2}]	*FF* [%]	*PCE*[a] [%]
1	GO (5 nm)	0.60	9.32	55.44	3.10 (2.95 ± 0.11)
2	G002-GO (5 nm)	0.60	10.21	63.17	3.87 (3.65 ± 0.19)
3	GO (6 nm)	0.59	9.17	49.72	2.69 (2.52 ± 0.13)
4	G002-GO (7 nm)	0.59	10.10	58.39	3.48 (3.28 ± 0.16)

[a]In the brackets are the average PCE values and standard deviations calculated from 10 devices.

3. CONCLUSION

Nanocomposites of two-dimensional rGO and GO can be utilized to effectively collect holes for PSCs. The composites can be prepared by directly dispersing rGO in aqueous solution of GO. GO can stabilize rGO in water through the interaction of its hydrophobic domain with rGO. This interaction leads to the quenching of the photoluminescence of GO by rGO. The addition of a small amount of rGO remarkably increases the conductivity of the GO films and effectively improves the photovoltaic efficiency of PSCs. The optimal rGO loading is 2 wt % with respect to GO in terms of the photovoltaic performance of the P3HT:PCBM PSCs. The optimal PCE for PSCs with G002-GO is 4.21%, which is comparable to that of commonly used PEDOT:PSS HCL. In addition, the small amount of rGO does not affect the chemical stability of GO matrix, leading to the enhancement in the device lifetime by more than 20 times compared to the control devices with PEDOT:PSS. The exploitation of the water-processed nanocomposites of two-dimensional rGO and GO as the hole-

collection material is a simple, green, and economic way to realize efficient and stable polymer solar cells.

4. EXPERIMENTAL SECTION

Materials and Preparation of GO/G_x-GO Solutions. P3HT and $PC_{60}BM$ were purchased from Rieke Metals and American Dye Source, respectively. Pristine GO aqueous solution (5.0 g L^{-1}) and high surface area reduced GO powder were purchased from Graphene Supermarket Corporation. All materials were used as received. GO solution was diluted to the required concentrations by adding deionized water. Corresponding amount of rGO was added into GO solution to prepare G_x-GO solution. GO and G_x-GO solutions were sonicated for 30 min using a VCX 130PB Probe Ultrasonic Homogenizer (130 kW × 80%).

Device Fabrication Process. The PSCs were fabricated by the following process. Patterned ITO glass substrates were sequentially cleaned with detergent, deionized water, acetone, and isopropyl alcohol. They were dried under nitrogen flow. After being treated with UV ozone in a Jelight UV−ozone cleaner for 15 min, the hole-collection layer was deposited by spin-coating a GO or G_x-GO aqueous solution at a speed of 2000 rpm for 40 s. The PEDOT:PSS layer was prepared by spin-coating a PEDO:PSS (Clevios P 4083) aqueous solution at a speed of 5000 rpm for 60 s. It was dried at 120 °C for 20 min. The ITO substrates coated with a hole-collection layer were then transferred into a glovebox filled with dried nitrogen gas. The active layer was prepared by spin-coating an *o*-DCB solution consisting of 20 g L^{-1} P3HT and 20 g L^{-1} PCBM at 600 rpm for 60 s. The P3HT:PCBM film was put in a covered Petri dish at room temperature, it dried after 60 min. The active layer had a thickness of around 200 nm. Finally, a 40 nm calcium layer and a 120 nm aluminum layer were successively deposited at a evaporating rate of 1.0 and 2−3 Å S^{-1}, respectively. The chamber pressure of the thermal evaporator was around 1.0×10^{-4} Pa. The PSCs were transferred into the glovebox and encapsulated with UV-curable epoxy and glass sheets. The PSCs were taken out for the photovoltaic tests in air. The active area of each PSC was 0.11 cm^2.

Measurement and Characterizations. Photoluminescent spectra were acquired with a Perkin Elmer LS55 fluorescence spectrometer. UV−vis transmittance spectra were taken with an Agilent Cary 5000 UV−vis−NIR instrument. AFM images were collected using a Veeco Nano Scope IV Multi-Mode AFM system in tapping mode. XPS and UPS were acquired with a VG ESCA 220i-XL system. The UV source was a He discharge lamp with a photon energy of 21.22 eV. The *J*−*V* curves of PSCs were measured with a computer-programmed Keithley 2420 source meter and a Newport's Oriel class A solar simulator, which simulated the AM1.5G sunlight (100 mW cm^{-2}) and certified to the JIS C 8912 standard. The light source was also calibrated with a standard silicon photodiode (Hamamatsu S1133).

AUTHOR INFORMATION

Corresponding Author

*E-mail: mseoj@nus.edu.sg.

Notes

The authors declare no competing financial interest.

ACKNOWLEDGMENTS

This work was financially supported by a research grant from the Agency for Science, Technology and Research (A* STAR) (R284-000-101-305).

REFERENCES

(1) He, Z.; Zhong, C.; Su, S.; Xu, M.; Wu, H.; Cao, Y. Enhanced Power-Conversion Efficiency in Polymer Solar Cells Using an Inverted Device Structure. *Nat. Photonics* **2012**, *6*, 591−595.

(2) You, J.; Dou, L.; Yoshimura, K.; Kato, T.; Ohya, K.; Moriarty, T.; Emery, K.; Chen, C.-C.; Gao, J.; Li, G.; Yang, Y. A Polymer Tandem Solar Cell with 10.6% Power Conversion Efficiency. *Nat. Commun.* **2013**, *4*, 1446−1455.

(3) You, J.; Chen, C.-C.; Hong, Z.; Yoshimura, K.; Ohya, K.; Xu, R.; Ye, S.; Gao, J.; Li, G.; Yang, Y. 10.2% Power Conversion Efficiency Polymer Tandem Solar Cells Consisting of Two Identical Sub-Cells. *Adv. Mater.* **2013**, *25*, 3973−3978.

(4) Wienk, M. M.; Kroon, J. M.; Verhees, W. J. H.; Knol, J.; Hummelen, J. C.; van Hal, P. A.; Janssen, R. A. J. Efficient Methano[70]fullerene/MDMO-PPV Bulk Heterojunction Photovoltaic Cells. *Angew. Chem., Int. Ed. Engl.* **2003**, *42*, 3371−3375.

(5) Padinger, F.; Rittberger, R. S.; Sariciftci, N. S. Effects of Postproduction Treatment on Plastic Solar Cells. *Adv. Funct. Mater.* **2003**, *13*, 85−88.

(6) Mühlbacher, D.; Scharber, M.; Morana, M.; Zhu, Z.; Waller, D.; Gaudiana, R.; Brabec, C. High Photovoltaic Performance of a Low-Bandgap Polymer. *Adv. Mater.* **2006**, *18*, 2884−2889.

(7) Blouin, N.; Michaud, A.; Leclerc, M. A. Low-Bandgap Poly(2,7-Carbazole) Derivative for Use in High-Performance Solar Cells. *Adv. Mater.* **2007**, *19*, 2295−2300.

(8) Liang, Y.; Xu, Z.; Xia, J.; Tsai, S.-T.; Wu, Y.; Li, G.; Ray, C.; Yu, L. For the Bright Future-Bulk Heterojunction Polymer Solar Cells with Power Conversion Efficiency of 7.4%. *Adv. Mater.* **2010**, *22*, E135−E138.

(9) Chu, T.; Lu, J.; Beaupr, S.; Zhang, Y. Bulk Heterojunction Solar Cells Using Thieno[3,4-c]pyrrole-4,6-Dione and Dithieno Silole Copolymer with a Power Conversion Efficiency of 7.3%. *J. Am. Chem. Soc.* **2011**, *133*, 4250−4253.

(10) Wang, N.; Chen, Z.; Wei, W.; Jiang, Z. Fluorinated Benzothiadiazole-Based Conjugated Polymers for High-Performance Polymer Solar Cells without Any Processing Additives or Post-Treatments. *J. Am. Chem. Soc.* **2013**, *135*, 17060−17068.

(11) Cui, C.; Wong, W.; Li, Y. Improvement of Open-Circuit Voltage and Photovoltaic Properties of 2D-Conjugated Polymers by Alkylthio Substitution. *Energy Environ. Sci.* **2014**, *7*, 2276−2284.

(12) Ye, L.; Zhang, S.; Zhao, W.; Yao, H.; Hou, J. Highly Efficient 2D-Conjugated Benzodithiophene-Based Photovoltaic Polymer with Linear Alkylthio Side Chain. *Chem. Mater.* **2014**, *26*, 3603−3605.

(13) He, Y.; Chen, H.-Y.; Hou, J.; Li, Y. Indene-C(60) Bisadduct: A New Acceptor for High-Performance Polymer Solar Cells. *J. Am. Chem. Soc.* **2010**, *132*, 1377−1382.

(14) Zhao, G.; He, Y.; Li, Y. 6.5% Efficiency of Polymer Solar Cells Based on Poly(3-Hexylthiophene) and Indene-C(60) Bisadduct by Device Optimization. *Adv. Mater.* **2010**, *22*, 4355−4358.

(15) Ross, R. B.; Cardona, C. M.; Guldi, D. M.; Sankaranarayanan, S. G.; Reese, M. O.; Kopidakis, N.; Peet, J.; Walker, B.; Bazan, G. C.; Keuren, V. E.; Holloway, B. C.; Drees, M. Endohedral Fullerenes for Organic Photovoltaic Devices. *Nat. Mater.* **2009**, *8*, 208−212.

(16) Li, G.; Shrotriya, V.; Huang, J.; Yao, Y.; Moriarty, T.; Emery, K.; Yang, Y. High-Efficiency Solution Processable Polymer Photovoltaic Cells by Self-Organization of Polymer Blends. *Nat. Mater.* **2005**, *4*, 864−868.

(17) Ma, W.; Yang, C.; Gong, X.; Lee, K.; Heeger, A. J. Thermally Stable, Efficient Polymer Solar Cells with Nanoscale Control of the Interpenetrating Network Morphology. *Adv. Funct. Mater.* **2005**, *15*, 1617−1622.

(18) Peet, J.; Kim, J. Y.; Coates, N. E.; Ma, W. L.; Moses, D.; Heeger, A. J.; Bazan, G. C. Efficiency Enhancement in Low-Bandgap Polymer Solar Cells by Processing with Alkane Dithiols. *Nat. Mater.* **2007**, *6*, 497−500.

(19) Zhang, F.; Jespersen, K. G.; Björström, C.; Svensson, M.; Andersson, M. R.; Sundström, V.; Magnusson, K.; Moons, E.; Yartsev, a.; Inganäs, O. Influence of Solvent Mixing on the Morphology and Performance of Solar Cells Based on Polyfluorene Copolymer/Fullerene Blends. *Adv. Funct. Mater.* **2006**, *16*, 667−674.

(20) Lai, Y. Y.; Shih, P. I.; Li, Y. P.; Tsai, C. E.; Wu, J. S.; Chen, Y. J.; Hsu, C. S. Interface Engineering to Enhance the Efficiency of Conventional Polymer Solar Cells by Alcohol-/Water-Soluble C-60 Materials Doped with Alkali Carbonates. *ACS Appl. Mater. Interfaces* **2013**, *5*, 5122−5128.

(21) Zhou, Y.; Fuentes-Hernandez, C.; Shim, J.; Meyer, J.; Giordano, A. J.; Li, H.; Winget, P.; Papadopoulos, T.; Cheun, H.; Kim, J.; Fenoll, M.; Dindar, A.; Haske, W.; Najafabadi, E.; Khan, T. M.; Sojoudi, H.; Barlow, S.; Graham, S.; Brédas, J. L.; Marder, S. R.; Kahn, A.; Kippelen, B. A Universal Method to Produce Low-Work Function Electrodes for Organic Electronics. *Science* **2012**, *336*, 327−332.
(22) Irwin, M. D.; Buchholz, D. B.; Hains, A. W.; Chang, R. P. H.; Marks, T. J. *p*-Type Semiconducting Nickel Oxide as an Efficiency-Enhancing Anode Interfacial Layer in Polymer Bulk-Heterojunction Solar Cells. *Proc. Natl. Acad. Sci. U. S. A.* **2007**, *105*, 2783−2787.
(23) Zhang, H.; Ouyang, J. High-Performance Inverted Polymer Solar Cells with Lead Monoxide-Modified Indium Tin Oxides as the Cathode. *Org. Electron.* **2011**, *12*, 1864−1871.
(24) He, Z.; Zhang, C.; Xu, X.; Zhang, L.; Huang, L.; Chen, J.; Wu, H.; Cao, Y. Largely Enhanced Efficiency with a PFN/Al Bilayer Cathode in High Efficiency Bulk Heterojunction Photovoltaic Cells with a Low Bandgap Polycarbazole Donor. *Adv. Mater.* **2011**, *23*, 3086−3089.
(25) Sun, K.; Zhao, B.; Murugesan, V.; Kumar, A.; Zeng, K.; Subbiah, J.; Wong, W. W. H.; Jones, D. J.; Ouyang, J. High-Performance Polymer Solar Cells with a Conjugated Zwitterion by Solution Processing or Thermal Deposition as the Electron-Collection Interlayer. *J. Mater. Chem.* **2012**, *22*, 24155−24165.
(26) Zhang, K.; Zhong, C. M.; Liu, S. J.; Mu, C.; Li, Z. K.; Yan, H.; Huang, F.; Cao, Y. Highly Efficient Inverted Polymer Solar Cells Based on a Cross-linkable Water-/Alcohol-Soluble Conjugated Polymer Interlayer. *ACS Appl. Mater. Interfaces* **2014**, *6*, 10429−10435.
(27) Sun, Y.; Takacs, C. J.; Cowan, S. R.; Seo, J. H.; Gong, X.; Roy, A.; Heeger, A. J. Efficient, Air-Stable Bulk Heterojunction Polymer Solar Cells Using MoO(x) as the Anode Interfacial Layer. *Adv. Mater.* **2011**, *23*, 2226−2230.
(28) Ma, D.; Lv, M.; Lei, M.; Zhu, J.; Wang, H.; Chen, X. Self-Organization of Amine-Based Cathode Interfacial Materials in Inverted Polymer Solar Cells. *ACS Nano* **2014**, *8*, 1601−1608.
(29) Kim, H. I.; Bui, T. T.; Kim, G. K.; Shin, W. S.; Park, T. A Benzodithiophene-Based Novel Electron Transport Layer for a Highly Efficient Polymer Solar Cell. *ACS Appl. Mater. Interfaces* **2014**, *6*, 15875−15880.
(30) Sun, K.; Zhao, B.; Kumar, A.; Zeng, K.; Ouyang, J. Highly Efficient, Inverted Polymer Solar Cells with Indium Tin Oxide Modified with Solution-Processed Zwitterions as the Transparent Cathode. *ACS Appl. Mater. Interfaces* **2012**, *4*, 2009−2017.
(31) Jeon, Y.-J.; Yun, J.-M.; Kim, D.-Y.; Na, S.-I.; Kim, S.-S. High-Performance Polymer Solar Cells with Moderately Reduced Graphene Oxide as an Efficient Hole Transporting Layer. *Sol. Energy Mater. Sol. Cells* **2012**, *105*, 96−102.
(32) Kemerink, M.; Timpanaro, S.; de Kok, M. M.; Meulenkamp, E. A.; Touwslager, F. J. Three-Dimensional Inhomogeneities in PEDOT:PSS Films. *J. Phys. Chem. B* **2004**, *108*, 18820−18825.
(33) Kim, Y.-H.; Lee, S.-H.; Noh, J.; Han, S.-H. Performance and Stability of Electroluminescent Device with Self-Assembled Layers of Poly(3,4-Ethylenedioxythiophene)−poly(styrenesulfonate) and Poly-electrolytes. *Thin Solid Films* **2006**, *510*, 305−310.
(34) Tan, Z.; Qian, D.; Zhang, W.; Li, L.; Ding, Y.; Xu, Q.; Wang, F.; Li, Y. Efficient and Stable Polymer Solar Cells with Solution-Processed Molybdenum Oxide Interfacial Layer. *J. Mater. Chem. A* **2013**, *1*, 657−664.
(35) Zilberberg, K.; Trost, S.; Schmidt, H.; Riedl, T. Solution Processed Vanadium Pentoxide as Charge Extraction Layer for Organic Solar Cells. *Adv. Energy Mater.* **2011**, *1*, 377−381.
(36) Chen, C.-P.; Chen, Y.-D.; Chuang, S.-C. High-Performance and Highly Durable Inverted Organic Photovoltaics Embedding Solution-Processable Vanadium Oxides as an Interfacial Hole-Transporting Layer. *Adv. Mater.* **2011**, *23*, 3859−3863.
(37) Steirer, K. X.; Ndione, P. F.; Widjonarko, N. E.; Lloyd, M. T.; Meyer, J.; Ratcliff, E. L.; Kahn, A.; Armstrong, N. R.; Curtis, C. J.; Ginley, D. S.; Ginley, D. S.; Berry, J. J.; Olson, D. C. Enhanced Efficiency in Plastic Solar Cells via Energy Matched Solution Processed NiOx Interlayers. *Adv. Energy Mater.* **2011**, *1*, 813−820.
(38) Lee, B. R.; Kim, J.; Kang, D.; Lee, D. W.; Ko, S.-J.; Lee, H. J.; Lee, C.-L.; Kim, J. Y.; Shin, H. S.; Song, M. H. Highly Efficient Polymer Light-Emitting Diodes Using Graphene Oxide as a Hole Transport Layer. *ACS Nano* **2012**, *6*, 2984−2991.
(39) Tan, Z.; Zhang, W.; Qian, D.; Cui, C.; Xu, Q.; Li, L.; Li, S.; Li, Y. Solution-Processed Nickel Acetate as Hole Collection Layer for Polymer Solar Cells. *Phys. Chem. Chem. Phys.* **2012**, *14*, 14217−14223.
(40) Gao, Y.; Yip, H.-L.; Hau, S. K.; O'Malley, K. M.; Cho, N. C.; Chen, H.; Jen, A. K.-Y. Anode Modification of Inverted Polymer Solar Cells Using Graphene Oxide. *Appl. Phys. Lett.* **2010**, *97*, 203306.
(41) Li, S.-S.; Tu, K.-H.; Lin, C.-C.; Chen, C.-W.; Chhowalla, M. Solution-Processable Graphene Oxide as an Efficient Hole Transport Layer in Polymer Solar Cells. *ACS Nano* **2010**, *4*, 3169−3174.
(42) Gao, Y.; Yip, H.-L.; Chen, K.-S.; O'Malley, K. M.; Acton, O.; Sun, Y.; Ting, G.; Chen, H.; Jen, A. K.-Y. Surface Doping of Conjugated Polymers by Graphene Oxide and Its Application for Organic Electronic Devices. *Adv. Mater.* **2011**, *23*, 1903−1908.
(43) Liu, J.; Kim, G.-H.; Xue, Y.; Kim, J. Y.; Baek, J.-B.; Durstock, M.; Dai, L. Graphene Oxide Nanoribbon as Hole Extraction Layer to Enhance Efficiency and Stability of Polymer Solar Cells. *Adv. Mater.* **2014**, *26*, 786−790.
(44) Liu, J.; Durstock, M.; Dai, L. Graphene Oxide Derivatives as Hole- and Electron-Extraction Layers for High-Performance Polymer Solar Cells. *Energy Environ. Sci.* **2014**, *7*, 1297−1306.
(45) Eda, G.; Chhowalla, M. Chemically Derived Graphene Oxide: Towards Large-Area Thin-Film Electronics and Optoelectronics. *Adv. Mater.* **2010**, *22*, 2392−2415.
(46) Guo, C. X.; Guai, G. H.; Li, C. M. Graphene Based Materials: Enhancing Solar Energy Harvesting. *Adv. Energy Mater.* **2011**, *1*, 448−452.
(47) Liu, J.; Xue, Y.; Gao, Y.; Yu, D.; Durstock, M.; Dai, L. Hole and Electron Extraction Layers Based on Graphene Oxide Derivatives for High-Performance Bulk Heterojunction Solar Cells. *Adv. Mater.* **2012**, *24*, 2228−2233.
(48) Murray, I. P.; Lou, S. J.; Cote, L. J.; Loser, S.; Kadleck, C. J.; Xu, T.; Szarko, J. M.; Rolczynski, B. S.; Johns, J. E.; Huang, J.; Yu, L.; Chen, L. X.; Marks, T. J.; Hersam, M. C. Graphene Oxide Interlayers for Robust, High-Efficiency Organic Photovoltaics. *J. Phys. Chem. Lett.* **2011**, *2*, 3006−3012.
(49) Yun, J.-M.; Yeo, J.-S.; Kim, J.; Jeong, H.-G.; Kim, D.-Y.; Noh, Y.-J.; Kim, S.-S.; Ku, B.-C.; Na, S.-I. Solution-Processable Reduced Graphene Oxide as a Novel Alternative to PEDOT:PSS Hole Transport Layers for Highly Efficient and Stable Polymer Solar Cells. *Adv. Mater.* **2011**, *23*, 4923−4928.
(50) Liu, X.; Kim, H.; Guo, L. J. Optimization of Thermally Reduced Graphene Oxide for an Efficient Hole Transport Layer in Polymer Solar Cells. *Org. Electron.* **2013**, *14*, 591−598.
(51) Liu, J.; Xue, Y.; Dai, L. Sulfated Graphene Oxide as a Hole-Extraction Layer in High-Performance Polymer Solar Cells. *J. Phys. Chem. Lett.* **2012**, *3*, 1928−1933.
(52) Kim, J.; Tung, V. C.; Huang, J. Water Processable Graphene Oxide:Single Walled Carbon Nanotube Composite as Anode Modifier for Polymer Solar Cells. *Adv. Energy Mater.* **2011**, *1*, 1052−1057.
(53) Thanh, T. T.; Ba, H.; Phuoc, L. T.; Nhut, J. M.; Ersen, O.; Begin, D.; Janowska, I.; Nguyen, D. L.; Grangerd, P.; Huu, C. P. A Few-Layer Graphene−Graphene Oxide Composite Containing Nano-diamonds as Metal-Free Catalysts. *J. Mater. Chem. A* **2014**, *2*, 11349−11357.
(54) Chen, R. F.; Knutson, J. R. Mechanism of Fluorescence Concentration Quenching of Carboxyfluorescein in Liposomes: Energy Transfer to Nonfluorescent Dimers. *Anal. Biochem.* **1988**, *172*, 61−77.
(55) Mei, X.; Ouyang, J. Ultrasonication-Assisted Ultrafast Reduction of Graphene Oxide by Zinc Powder at Room Temperature. *Carbon* **2011**, *49*, 5389−5397.
(56) Girtan, M.; Rusu, M. Role of ITO and PEDOT:PSS in Stability/Degradation of Polymer:Fullerene Bulk Heterojunctions Solar Cells. *Sol. Energy Mater. Sol. Cells* **2010**, *94*, 446−450.

(57) Norrman, K.; Madsen, M. V.; Gevorgyan, S. A.; Krebs, F. C. Degradation Patterns in Water and Oxygen of an Inverted Polymer Solar Cell. *J. Am. Chem. Soc.* **2010**, *132*, 16883−16892.
(58) Park, Y.; Choong, V.; Gao, Y.; Hsieh, B. R.; Tang, C. W. Work Function of Indium Tin Oxide Transparent Conductor Measured by Photoelectron Spectroscopy. *Appl. Phys. Lett.* **1996**, *68*, 2699−2701.